Hindawi
Mathematical Problems in Engineering
Volume 2023, Article ID 6899076, 15 pages
https://doi.org/10.1155/2023/6899076

Research Article

RIS-Assisted Coverage Optimization for 5G-R Channel in Station Scenario Based on ML and RT

Bin Lu,[1] **Xinghai Guo**,[2] **Xinyi Shan**,[2] **and Fang Li**[3]

[1]*China Telecom Research Institute, Guangzhou 510630, China*
[2]*School of Electronic and Information Engineering, Beijing Jiaotong University, Beijing 100044, China*
[3]*Guangzhou Maritime University, Guangzhou 510700, China*

Correspondence should be addressed to Fang Li; fanglee.whut@gmail.com

Received 19 October 2022; Revised 15 March 2023; Accepted 26 April 2023; Published 6 June 2023

Academic Editor: Ardashir Mohammadzadeh

As one of the most important radio communication scenarios in vertical industry, the high-speed railway (HSR) station is facing the challenge of coverage optimization due to its complex structure. Regarding the wireless network planning and optimization of HSR stations as a part of the customized network, this paper makes an analysis on the 5G-R channel in the HSR station scenario. Channel characteristics, including path loss, power ratio (PR), and angular spread (AS), are extracted on the basis of ray tracing (RT). Multipath components can also be distinguished based on RT. In order to achieve a better performance, the reconfigurable intelligent surface (RIS) technology is adopted to the network deployment. Moreover, machine learning (ML) is used to locate the best direction of the beam. The analysis results show that the received power in RIS-assisted channels is significantly promoted. Our research can provide a deep understanding to the 5G-R channel in station scenario and a well reference for the design and optimization of the customized network.

1. Introduction

From 2019, global operators began to deploy 5G networks and 5G customized networks commercially. The 5G customized network is the best practice private network for cloud network integration and the network foundation for accelerating the digital transformation of thousands of businesses.

High-speed railway (HSR) station is an important part of the railway transportation system as well as one of the important scenarios of the 5G customized network. The construction of "smart railway station" needs the solid support of an efficient and stable wireless communication network, which can provide a high speed data transmission and satisfactory passenger service. However, the current global system for mobile communications railway (GSM-R) system suffers insufficient bearing capacity and serious band interference problems [1]. As a development of the mobile communication technology, the fifth-generation communication (5G) can meet the requirements such as high reliability and low latency. Thus, the 5G-railway (5G-R) communication system will be an evolutionary option for the next-generation railway communication [2].

In the existing research, most of the efforts made on the HSR scenarios focus on urban scenario [3], rural scenario [4], tunnels [5], and crossing bridges [6]. Due to the different structural features from the aforementioned scenarios, HSR station scenarios generally include metallic surfaces of train bodies, railway equipment, and other devices. This will make different channel characteristics distinguished from other scenarios [7]. Therefore, the existing statistical models cannot be applied to predict the coverage inside the station directly.

Generally, lots of methods have been studied for channel modeling. Ray tracing (RT) is one of the most popular deterministic modeling methods, which can be used to describe the wave propagation in this scenario [8]. The RT method can abstract the electromagnetic waves with various propagation mechanisms into the light-like rays [9]. Since the reflection paths can be extracted through RT simulations,

it is technically practical to use the reconfigurable intelligent surface (RIS) to change channel characteristics to optimize the coverage [10], which can meet challenges of the coverage optimization caused by the high frequency band and large path loss in the 5G-R system [11].

As a passive device, RIS can improve the channel without introducing other interference, so it has attracted extensive attention in the research [12, 13]. RIS is a two-dimensional structure with a large number of reflective elements, which can induce an adjustable independent shift on the incident signal [14, 15]. Thus, RIS is suitable for enhancing the coverage in key regions at a low cost [16]. A large number of studies have been conducted using RIS for coverage optimization. In [17], the cell coverage is maximized by optimizing the RIS orientation and horizontal distance. The RIS-assisted channel model is presented in [18], and the principle of phase-shift adjustment at RIS beamforming is applied to enhance the coverage in desired regions [19]. The RIS can be programmed to discrete adjustment of the reflection phase [20], which provides an opportunity for the introduction of various artificial intelligence methods.

In the existing studies, there are two main ideas for the optimization of RIS. The first one is to calculate the RIS-assisted channel model and optimize the required parameters [17, 21, 22]. The calculation of this case is accurate, but it is difficult to apply to large and complex systems. The second idea is to use machine learning methods, including deep learning (DL) and reinforcement learning (RL), to solve the required parameters [23, 24]. Moreover, in relevant studies, the authors in [25] propose that the communication system can be abstracted as a fuzzy system. The artificial neural networks (ANNs) can be built to optimize the parameters of the complex communication system [26].

In this paper, the 5G-R wireless network planning and optimization for HSR stations are conducted, which are assisted by the RIS technology and ML algorithm for the best direction orientation of the beam. The extraction of 5G-R channel characteristics is achieved by the RT technology. The main contributions of this paper are as follows:

(1) High precision reproduction of wireless signal propagation in HSR station scenario and channel characteristics extraction based on RT platform are conducted. Focusing on the complex structure, we build the physical model of the HSR station. Considering the rich multipath components of the radio propagation in the HSR station, we analyze the distribution and sources of electromagnetic waves using RT platform.

(2) RIS-assisted wireless network planning and optimization for HSR station scenario are designed. The deployment of the wireless network is mainly based on traversal iteration with high cost and low efficiency. We thus adopt the RIS technology to obtain a better design, which can improve network coverage with a low cost.

(3) The best beam orientation of RIS based on the ML algorithm is realized. In order to obtain the best radiation direction, we use the ML algorithm to locate the best direction of the beam. Thus, with the combination of RIS and ML, wireless coverage can be efficiently and accurately planned and optimized for the HSR station scenario.

The rest of the paper is organized as follows: Section 2 introduces the RT configuration. Section 3 analyzes channel parameters and proposes the advice. Finally, we draw the conclusion in Section 4.

2. Ray-Tracing Simulations

A high-performance computing cloud-based platform named CloudRT is applied to simulate the wave propagation inside the HSR station [9]. The CloudRT architecture can be described as the structure in Figure 1. A typical HSR station scenario is reconstructed as shown in Figure 2(a). The model consists of ground, railway, platform, awning, columns, and electric traction racks. Surfaces of these scatterers are presented in the figure. The material's electromagnetic (EM) parameters at 2.1 GHz band of different parts are listed in Table 1. As one of popular deterministic channel modeling methodologies, ray tracing can provide various channel parameters, including channel transfer function (CTF), center frequency, number of multipaths, multipath components (MPCs) properties, received signal level (RSL), and physical environment information for each TX-RX link. The CTF can be transformed to channel impulse response (CIR) by inverse Fourier transform, from which the power delay profile (PDP), delay spread, power ratio, Doppler spread, etc., can be extracted. The small-scale channel characteristics in power, delay, and frequency domains can thus be characterized. Moreover, for the space domain, the multipath characteristics, containing comprehensive data of the MPCs, including type (i.e., LOS or NLOS path), bounces, delay, transmission distance, electric field strength, transmission loss, angle of arrival (AOA), elevation angle of arrival (EOA), angle of departure (AOD), and elevation angle of departure (EOD) can be obtained as well. For the large-scale channel characteristics, the path loss and shadow fading can be obtained from the RSL and physical environment information which consist of snapshot index, time, TX position, and RX position. Consequently, we can depict the radio channel for the HSR station scenario from multiple dimensions by exploiting RT simulation.

As shown in Figure 2(b), the simulation is carried out on 8 railway lines marked by the red box. The RX is deployed on the top of a HSR train. Simulation is performed every 10 m of movement as the train moves along the selected railway lines. The TX is deployed on the side of the station. The TX and RX adopt directional antenna and omnidirectional antenna, respectively, and their antenna patterns are exhibited in Figure 3.

In order to ensure accurate simulation results as well as efficient computation, a presimulation is conducted to determine the maximum reflection order. The contribution of each order of reflection is calculated via RT simulations with reflected rays up to the 2nd order in Figure 4.

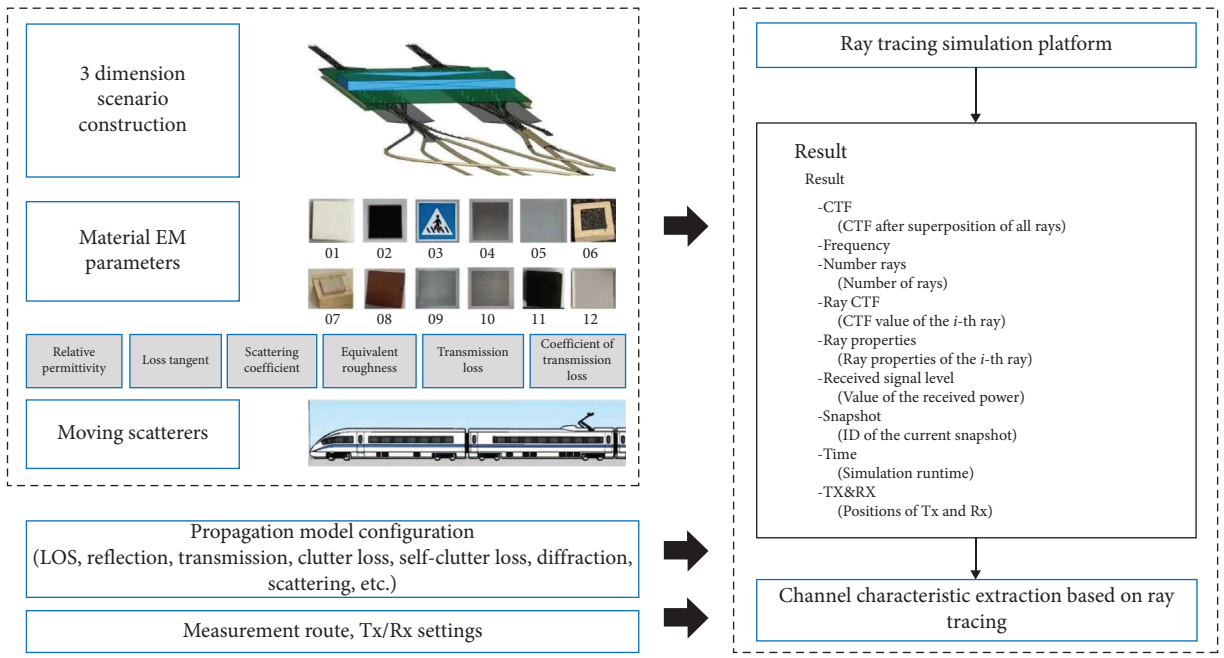

Figure 1: CloudRT architecture.

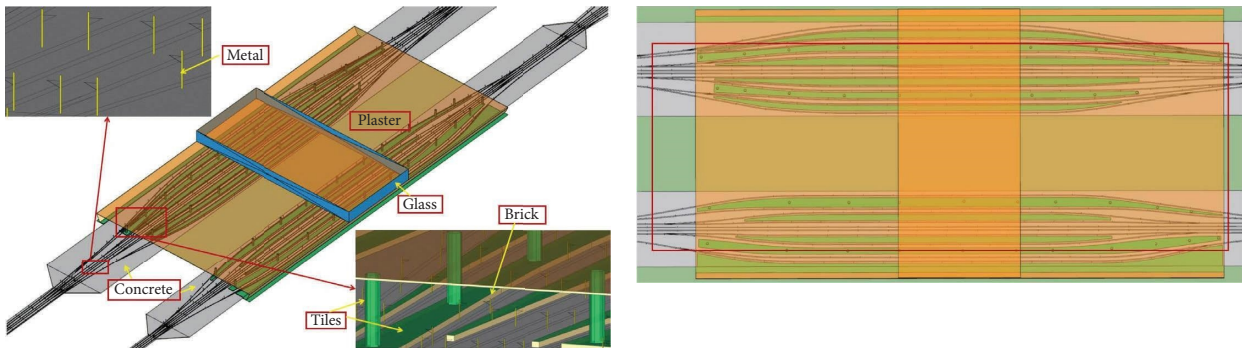

Figure 2: (a) Model of HSR station scenario. (b) Simulation region.

Table 1: EM properties of materials at 2.1 GHz.

Material	ϵ_r'	$\tan\delta$
Metal	1.000	10^6
Glass	6.270	0.140
Brick	3.750	0.091
Concrete	5.310	0.097
Tiles	6.275	0.030
Plaster	2.940	0.058

It can be seen from the power percentage of every order that there is no essential difference between the 1st order and the 2nd order of reflection. Thus, the maximum simulation reflection order is determined as the 1st order. The detailed configuration is listed in Table 2. Simulations are conducted after completing the relevant configurations. One of the snapshots of RT simulation is exhibited in Figure 5, where the yellow sphere and green sphere represent the location of TX and RX, respectively.

3. Channel Characterization of the Original Channel

In this section, the scenario is divided into the LOS region and the NLOS region. The channel characteristics, including path loss model and angular spread, are analyzed based on the simulation results. Moreover, the coverage inside the station is presented.

3.1. Path Loss Modeling. The simulated and fitted curves of path loss with distance are shown in Figure 6. It can be seen from the figures that the path loss models of both LOS and NLOS regions of the HSR station obey the A-B model as follows:

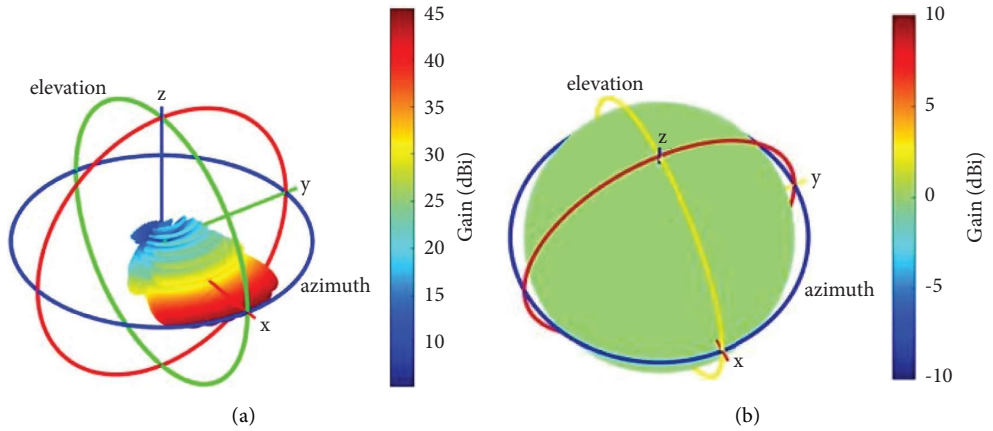

Figure 3: Antenna gain patterns of (a) TX antenna and (b) RX antenna.

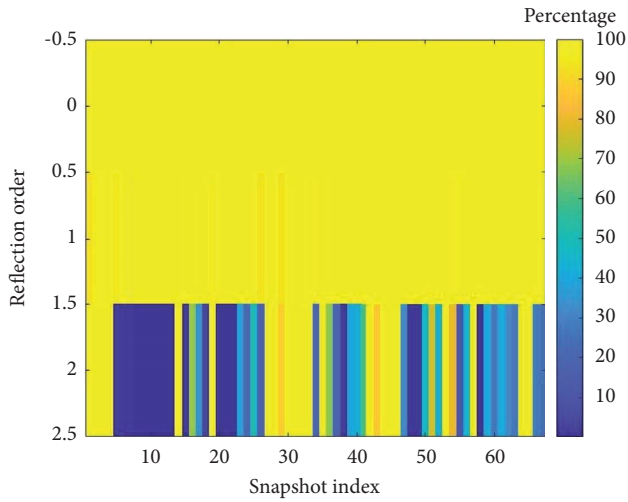

Figure 4: Power distribution of every order reflection.

Table 2: Configuration of RT simulations.

Item	Configuration
Center frequency	2.1 GHz
Bandwidth	10 MHz
Subcarrier interval	15 kHz
TX antenna type	Vertical polarized directional
RX antenna type	Vertical polarized omnidirectional
TX antenna gain	0 dBi
RX antenna gain	0 dBi
TX height	45 m above the ground
TX power	43 dBm
RX height	0.49 m above the train
Train height	4.5 m

$$PL = A \times 10 \times \log_{10} d + B + X_{\sigma}, \tag{1}$$

where PL denotes the path loss in dB. d is the distance between TX and RX in meters. A and B represent the slope and intercept of the model, respectively. X_{σ} is a Gaussian random variable with a mean of 0 and standard deviation of σ. The parameters in equation (1) are estimated based on the simulation results according to the nonlinear least squares principle as listed in Table 3. The results show that the path loss exponents are 6.77 and 3.99 in the LOS and NLOS regions, respectively.

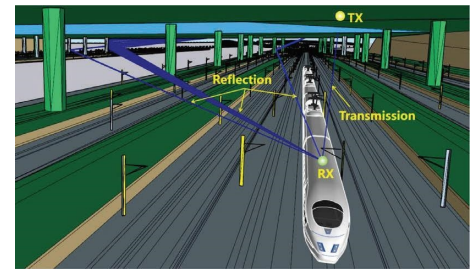

Figure 5: One snapshot of RT simulations.

3.2. Angular Spread. The angular spread is an important characteristic to indicate the channel selective fading in the spatial domain [27], which is one of the references of antenna deployment type in space [28]. Azimuth angular spread of arrival (ASA), azimuth angular spread of departure (ASD), elevation angular spread of arrival (ESA), and elevation angular spread of departure (ESD) are calculated through the same approach of 3GPP protocol [29] as follows:

$$\sigma_{\mathrm{AS}} = \sqrt{\frac{\Sigma_{n=1}^{N}\left(\theta_{n,\mu}^{2} P_n\right)}{\Sigma_{n=1}^{N} P_n}}, \tag{2}$$

where σ_{AS} represents the angular spread. P_n represents the power of the n-th multipath. N denotes the number of multipaths received by receivers. The values of N and P_n are stored in the RT simulation results. $\theta_{n,\mu}$ is defined by

$$\sigma_{n,\mu} = \mathrm{mod}\ \left(\theta_n - \mu_\theta + \pi, 2\pi\right) - \pi, \tag{3}$$

where θ_n represents the azimuth/elevation angle of arrival/departure (AoA, AoD, EoA, and EoD) of the n-th multipath, which can be obtained in the dataset of simulation results. μ_n is calculated by

Table 3: Parameters for the fitted model.

Area	A	B	σ
LOS	6.77	−71.94	7.93
NLOS	3.99	−2.96	7.27

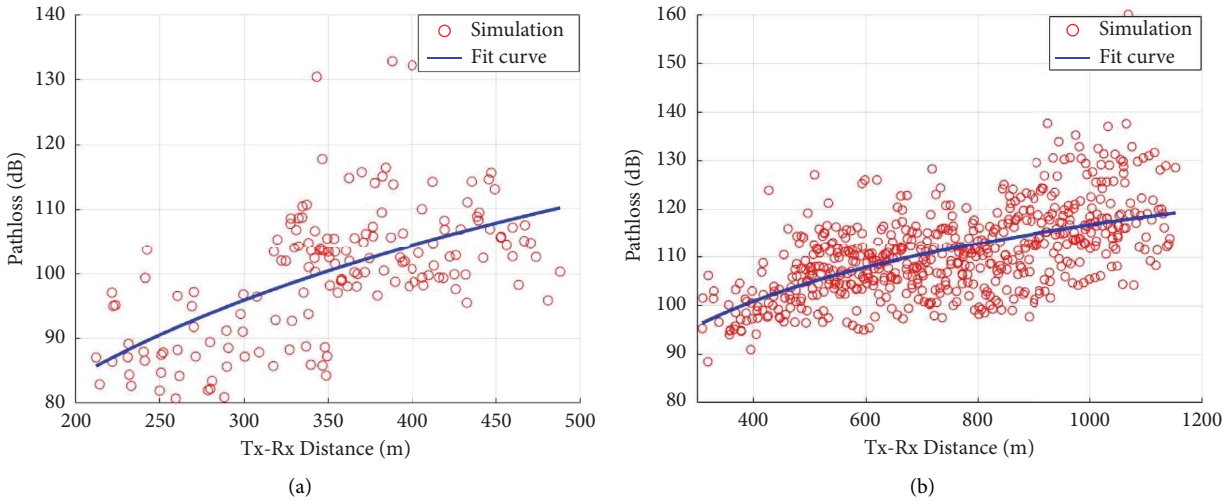

Figure 6: Path loss in (a) LOS region and (b) NLOS region.

$$\mu_\theta = \frac{\Sigma_{n=1}^{N} \theta_n P_n}{\Sigma_{n=1}^{N} P_n}. \tag{4}$$

Figures 7 and 8 show the cumulative density functions (CDFs) of the angular spread in LOS and NLOS regions, respectively. The mean values and standard deviations of the four angular spreads in both regions are shown in Table 4, in which μ and σ represent the mean value and the standard deviation, respectively.

From the table, it can be concluded that the overall ASs of the channel in the LOS region are higher than those in the NLOS region. This is due to the fact that the LOS region usually distributes in the open region of the scenario, where multipaths can come from all directions. Thus, the angles between multipaths and the main path are larger. The low height of the scatter in this scenario makes the arrival and departure angles in elevation plane smaller. Consequently, the ASs in the elevation plane are lower than those in the azimuth plane.

3.3. Power Ratio. The power ratio (PR) is defined as the ratio between the power of the strongest path and the sum of the power of the rest paths. This value is generally described as Rician K-factor in the LOS region. The PR [30] is calculated by

$$\mathrm{PR}[\mathrm{dB}] = 10 \log_{10}\left(\frac{P_{\mathrm{strongest}}}{P_{\mathrm{rest}}}\right), \tag{5}$$

where PR denotes the power ratio in dB. $P_{\mathrm{strongest}}$ and P_{rest} represent the power of the strongest path and the sum of rest paths in mW, respectively. The CDFs of PR in both LOS and NLOS regions are illustrated in Figure 9. It can be found that the mean values of the PR in the LOS and NLOS regions are 5.31 dB and 6.94 dB, respectively.

3.4. SS-RSRP Coverage. The SS-RSRP is defined as the linear average over the power contributions (in mW) of the resource elements (REs) that carry secondary synchronization signals (SS). The SS-RSRP can be calculated by subtracting the path loss from the transmitting power per RE. For 5G-R system, the transmitting power per RE can be calculated by

$$P_{\mathrm{r}} = \frac{P_{\mathrm{T}} \times N_{\mathrm{c}}}{N_{\mathrm{RB}} \times 12}, \tag{6}$$

where P_{r} denotes the transmitting power per RE. P_{T} is the transmitting power per channel. N_{c} is the number of channels. N_{RB} means the number of resource blocks, which equals 51 in this configuration. According to equation (6), the transmitting power per RE is 31.55 dBm. The SS-RSRP of each receiving point in this scenario is then derived and illustrated in Figure 10. According to our investigation in China Mobile Communication Corporation (CMCC), the SS-RSRP threshold is set as −95 dBm. In coverage planning, no more than 5% of the receiving region can be below this threshold. The receiving points with SS-RSRP below and above the threshold are defined as the weak and strong regions as shown in Figure 10. In this situation, a total of 40 receiving points have SS-RSRP below −95 dBm, failing to meet the standard.

From the result shown in Figure 10, it can be found that the coverage in the NLOS region is not very satisfactory. However, Figure 8 shows that the angle spreads are relatively

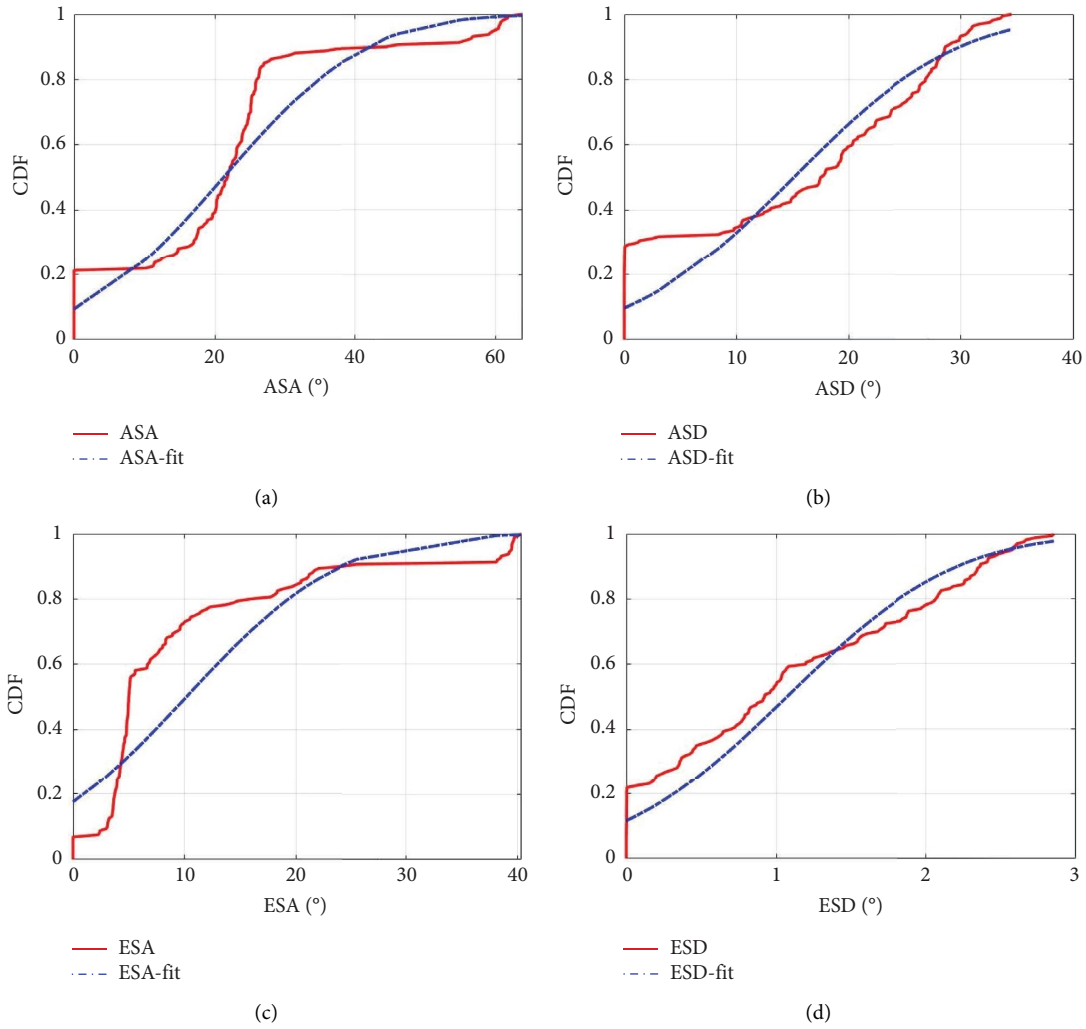

Figure 7: Angular spread in the LOS region. (a) ASA. (b) ASD. (c) ESA. (d) ESD.

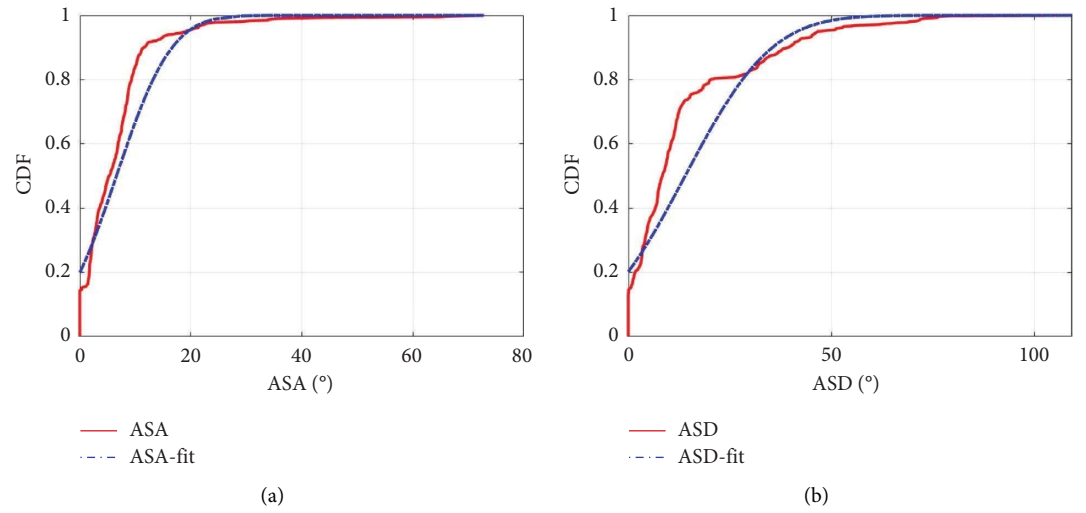

Figure 8: Continued.

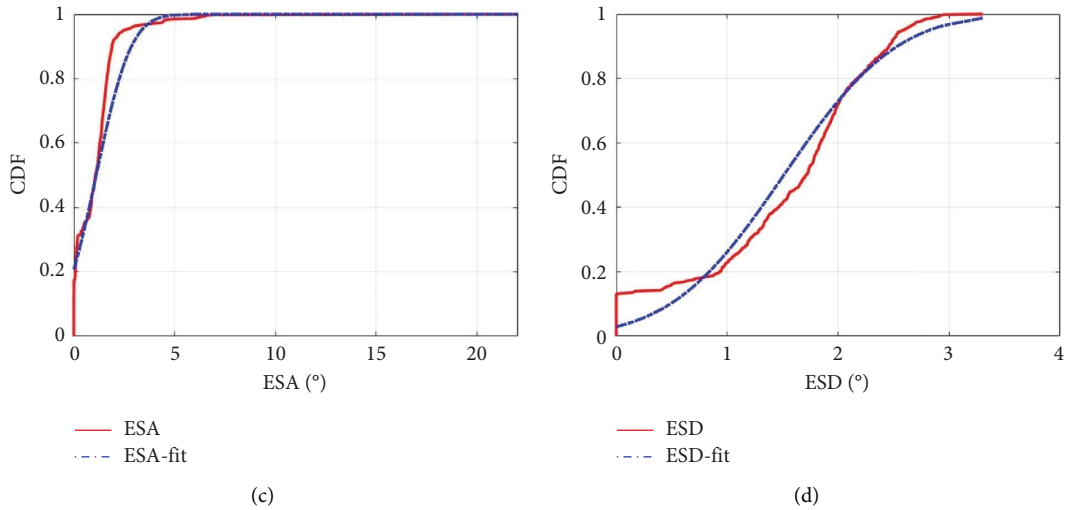

Figure 8: Angular spread in the NLOS region. (a) ASA. (b) ASD. (c) ESA. (d) ESD.

Table 4: EM properties of materials at 2.1 GHz.

	LOS	NLOS
μ_{ASA}	21.17°	6.60°
σ_{ASA}	16.06°	7.83°
μ_{ASD}	15.08°	13.99°
σ_{ASD}	11.61°	16.78°
μ_{ESA}	10.18°	1.11°
σ_{ESA}	10.89°	1.36°
μ_{ESD}	1.07°	1.51°
σ_{ESD}	0.89°	0.80°

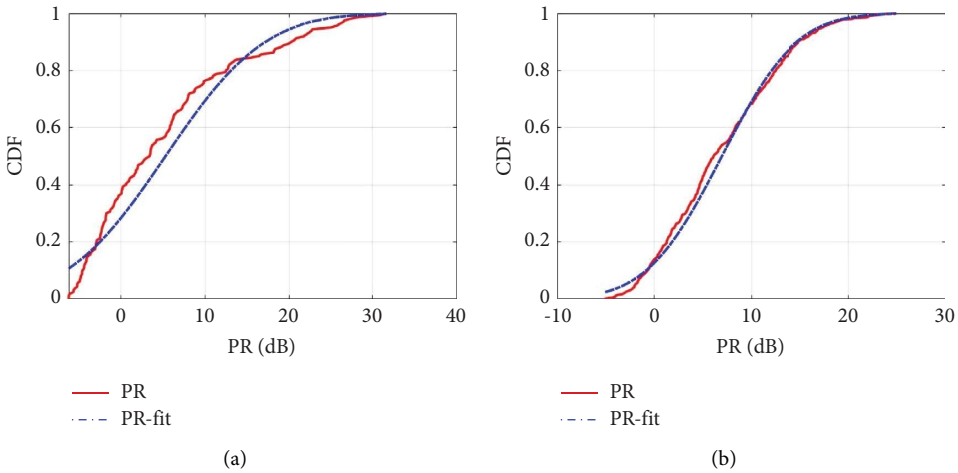

Figure 9: PR in the LOS and NLOS regions (a) LOS region. (b) NLOS region.

concentrated. Thus, the RIS can be deployed to enhance the coverage.

4. Model of RIS-Assisted Channel

4.1. RIS Beamforming. The geometric structure of the RIS is defined as a $M \times N$ array, as shown in Figure 11.

In the structure, the geometric center of the RIS is set to the origin of the Cartesian coordinate system. The RIS is placed on the x-y plane, with each row parallel to the x axis and each column parallel to the y axis. The location of the unit can be represented as

$$L_{m,n} = \left(\left(n - \frac{N+1}{2}\right)dx, \left(\frac{M+1}{2} - m\right)dy, 0\right), \tag{7}$$

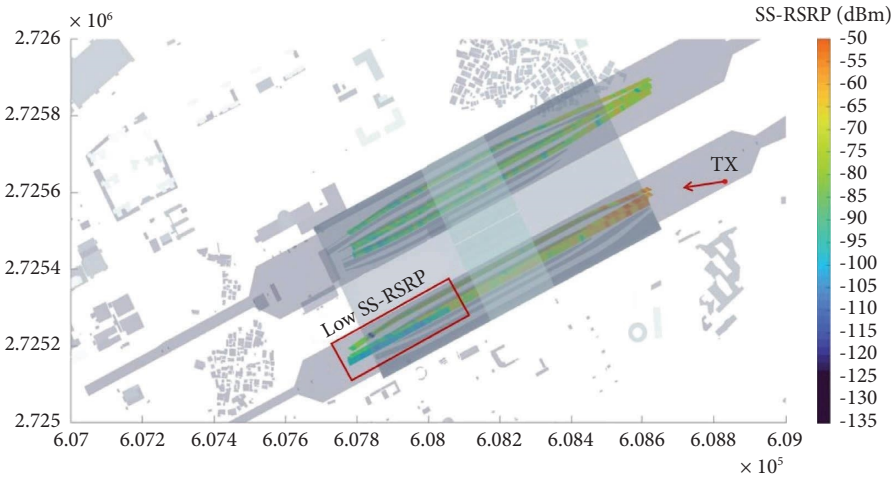

Figure 10: Coverage of the original channel.

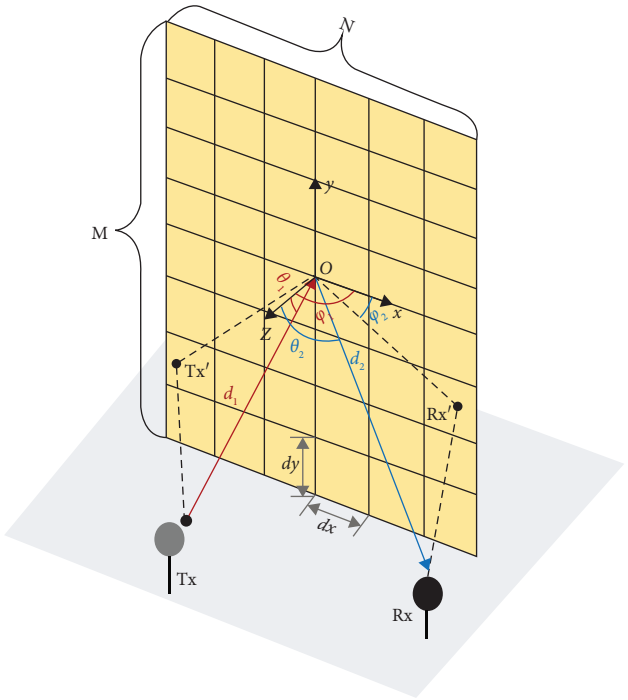

Figure 11: RIS schematic.

where dx and dy are the width and length of the unit, respectively.

We use the spherical coordinate system (d, θ, ϕ) to express the positions of TX and RX. (d_1, θ_1, ϕ_1) and (d_2, θ_2, ϕ_2) represent the locations of TX and RX, respectively, viewed from the geometric center of the RIS plane. θ is the zenith angle, which means the angle between the ray and the plane xOz. ϕ represents the azimuth angle, i.e., the angle between the projection of the ray on the plane xOz and the x axis.

To simulate the RIS gain in the radio channel, this paper will employ the beamforming pattern generation method for multiple-input multiple-output (MIMO) system based on the 3GPP 37.840 protocol. The detailed generation process is as follows:

$$\begin{aligned} 20 \times \log_{10} P_{\mathrm{E}}(\theta, \phi) &= G_{\mathrm{E,Max}} - \min\Big(-A_{\mathrm{E,H}}(\phi) \\ &\quad + A_{\mathrm{E,V}}(\theta), \mathrm{A_m}\Big), \\ A_{\mathrm{E,H}}(\phi) &= -\min\left[12\left(\frac{\phi}{\phi_{3\mathrm{dB}}}\right)^2, \mathrm{A_m}\right], \\ A_{\mathrm{E,V}}(\theta) &= -\min\left[12\left(\frac{\phi - 90}{\phi_{3\mathrm{dB}}}\right)^2, \mathrm{SLA_v}\right], \end{aligned} \tag{8}$$

where $P_{\mathrm{E}}(\theta, \phi)$ is the amplitude value of radiation unit pattern. $G_{\mathrm{E,Max}}$ denotes the maximum directional gain of the radiation element. $A_m = 30\,\mathrm{dB}$ is the front-to-back ratio of the beam. $A_{\mathrm{E,H}}(\phi)$ and $A_{\mathrm{E,V}}(\theta)$ are the horizontal and vertical radiation patterns of the radiation unit. $\phi_{3\mathrm{dB}}$ and $\theta_{3\mathrm{dB}}$ are the horizontal and vertical 3 dB beam width. $\mathrm{SLA_v}$ is the sidelobe limit.

$$\begin{aligned} v_{n,m} = \exp\Bigg(i \cdot 2\pi\Bigg(&(m-1) \cdot \frac{dy}{\lambda} \cdot \sin(\theta_{\mathrm{etilt}}) \\ &+ (n-1) \cdot \frac{dx}{\lambda} \cdot \sin(\theta_{\mathrm{etilt}}) \cdot \sin(\phi_{\mathrm{escan}})\Bigg)\Bigg), \end{aligned} \tag{9}$$

where $v_{n,m}$ represents the unit spacing of the $m \times n$ antennas array. λ is the wavelength. $\theta_{\mathrm{etilt}} \in [-90^\circ, 90^\circ]$ and $\theta_{\mathrm{escan}} \in [0^\circ, 180^\circ]$ denote the electric dip angle and the horizontal steering angle, respectively.

$$w_{n,m} = \frac{1}{\sqrt{MN}} \exp\left(i \cdot 2\pi \left((m-1) \cdot \frac{dy}{\lambda} \cdot \sin\left(\theta_{\text{etilt}}\right) + (n-1) \cdot \frac{dx}{\lambda} \cdot \sin\left(\theta_{\text{etilt}}\right) \cdot \sin\left(\phi_{\text{escan}}\right) \right) \right), \tag{10}$$

where $w_{n,m}$ represents the unit weight of the $M \times N$ antennas array. $\sqrt{MN}/1$ is the normalization coefficient.

Based on the equations mentioned above and the 3GPP 37.840 protocol, we can set up the corresponding variable parameters given in Table 5 and obtain the beam pattern as shown in Figure 12.

4.2. PSO Algorithm. According to the 2.1 GHz center frequency of the 5G-R communication, the wave length equals 0.14 m. Therefore, the size of the 16×16 RIS is 1.25 square meters. The aforementioned beam pattern generation methodology indicates that the elevation angle and azimuth angle of the pattern correspond to a combination of weight coefficients for each of element in the $M \times N$ array. Although the active RIS can adjust the weight coefficients adaptively in terms of the channel estimation outcomes from base station, relatively fixed weight coefficients for each deployment position will be more practical in industry. We thus propose to determine the beam pattern direction based on RT space domain outcomes. After that, the beam pattern direction will be treated as RIS pattern direction in the following radio coverage enhancement. Figure 13 exhibits one of surfaces which have multiple reflection and scattering phenomena in the station scenario. The surface with 1.2 square meters is on the wall of the station. Multiple reflection paths and scattering paths with different powers influence the RSLs of the corresponding RX positions on the railway lines. Taking the mentioned surface above as an example, the particle swarm optimization (PSO) algorithm will find an optimal RIS pattern direction to replace the reflection paths and scattering paths. As one of common machine learning algorithms, the PSO is a computational method that optimizes a problem by iteratively trying to improve a candidate solution with regard to a given measure of quality. The optimal RIS pattern direction based on PSO outcomes will increase the RSLs of the RX positions which are affected by the reflection paths and scattering paths.

The RIS 3-dB beamwidth in azimuth plane and elevation plane equals to 15° and 12°, respectively. Therefore, we set an ellipse in the space domain to express the longitudinal section of the RIS pattern (see Figure 13).

The angular information of the RIS pattern direction is in the viewpoint of the surface deployed by the RIS. The objective function of the PSO algorithm aims to select an angle of the RIS pattern direction to obtain maximum multipaths energy contained in the ellipse, as given as follows:

$$\text{argmax} \sum_{k=0}^{K_T} 10 \cdot \log_{10}\left[P_{\text{RIS}}\left(Az_k, El_k\right)\right], \tag{11}$$

Table 5: Parameters of beam pattern.

Parameters	Value
$M \times N$	16×16
dx, dy	$\lambda/2$
Frequency	2.1 GHz
$\phi_{3\text{dB}}$	4.2°
$\theta_{3\text{dB}}$	4.2°

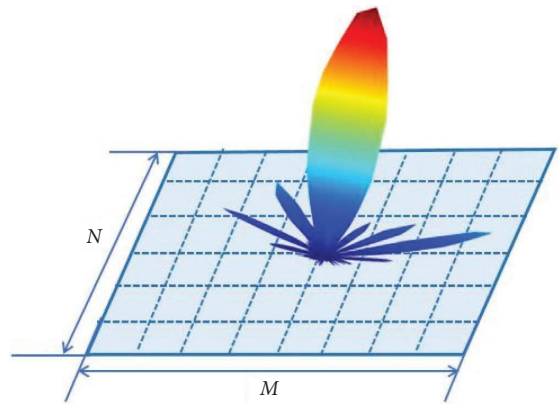

Figure 12: RIS beamforming.

where $P_{\text{RIS}}(Az_k, El_k)$ represents the power of the RIS pattern. K_T denotes total numbers of the scattering and reflection paths on the RIS. Az_k and El_k express the azimuth angle and elevation angle of the k-th path, respectively. Afterwards, the multipaths energy will be enhanced by the RIS gain. The angular granularities for the circular center adjustment in azimuth plane and elevation plane are infinitesimal in the mathematical aspect. Many candidate circular centers will appear. Owing to many candidates of the RIS pattern direction, the PSO can acquire the optimal RIS pattern direction in accordance with the algorithm structure diagram shown in Figure 14.

Here, the PSO algorithm exploits 100 swarms. The minimum and maximum azimuth angles are 0° and 180°, respectively. On the other hand, the minimum elevation angle equals to −90°, while the maximum elevation angle equals to 90°. The rand(·) is in Figure 14. w denotes stochastic variable which meets uniform distribution on [0, 1]. The Az_p represents the azimuth angle of the p-th particle. The El_p represents the elevation angle of the p-th particle. Moreover, we define the Az_p' and El_p' as the swarm's best known outcomes of the last iteration. The D_{ang} expresses the difference between two adjacent iteration outcomes as

$$D_{\text{ang}} = \sqrt{\left(Az'_{\text{gbest}} - Az_{\text{gbest}}\right)^2 + \left(El'_{\text{gbest}} - El_{\text{gbest}}\right)^2}. \tag{12}$$

The $THR_c = 3$ in Figure 14 represents the threshold of convergence determination. The factor A_{cc} will accumulate one if the difference of two adjacent iteration outcomes D_{ang} is lower than 0.5. Otherwise, the factor A_{cc} will turn to zero. To limit the PSO iteration, the maximum iteration $\max_{\text{iter}} = 50$ is configured. Moreover, the inertia weight is 0.8. Both of the acceleration constants, c_1 and c_2, equal 1.5. Table 6 lists

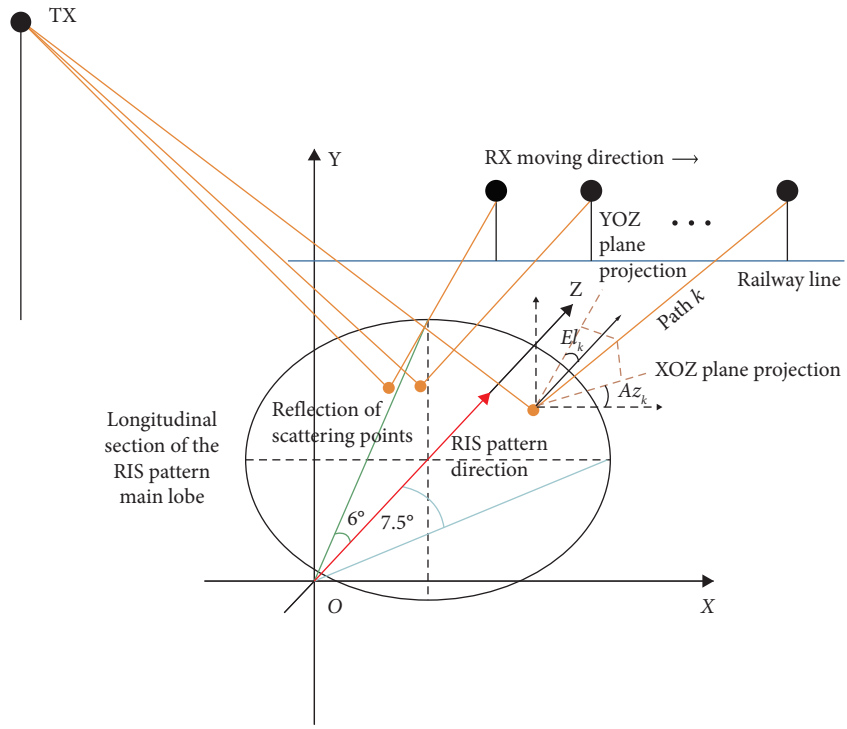

Figure 13: Longitudinal section of the RIS pattern.

the detailed PSO parameters configuration. On the basis of the PSO algorithm, Figure 15 shows the iteration outcomes.

Figure 15 illustrates the PSO outcomes which have completed convergence after 16 iterations. Since the station scenario contains many regions deploying the RIS, we employ the PSO algorithm to determine the RIS pattern direction based on space domain channel properties extraction. Consequently, a relatively fixed weight coefficient for each deployment position of the RIS will be obtained.

4.3. Comparison and Analysis. The following content will exhibit the results on the radio coverage enhancement for the station scenario. Figure 16 presents the SS-RSRP of the RIS-assisted channel. The result shows that the RIS will bring a good coverage improvement.

Figure 17 exhibits the path loss comparison between the RIS-assisted channel and the original channel. After deploying the RIS, the path loss has a significant decrease in the region with multipaths enhanced by RIS.

On the other hand, the paper also considers other optimization methods in practice. According to our investigation, manual antenna direction adjustment is a common method for radio coverage optimization coverage in practical engineering application. The antenna rotation direction is manually adjusted in terms of the weak coverage region of the scenario.

In the original channel, the TX directional antenna points to the center of the scenario. As shown in the Figure 10, the weak coverage points that the SS-RSRP fails to meet the −95 dBm and is mainly concentrated at the red rectangle region. Thus, the antenna will be rotated to face the red rectangle region. Figure 18 exhibits that the antenna is rotated 12° counterclockwise and raised 1° vertically to obtain a better radio coverage. The corresponding coverage heatmap is shown in Figure 18.

In this case, there are 37 weak coverage points, which represents a 7.5% reduction in weak coverage.

Manual adjustment of the antenna direction is difficult to acquire an optimal radio coverage optimization outcome. The ergodic method of antenna direction will provide an idea to find the relatively appropriate azimuth angles and elevation angles of the antenna. On the basis of RT simulation, the ergodic method will obtain radio coverages in each preset angle. For the azimuth angle, the antenna is rotated horizontally from 60° counterclockwise to 30° clockwise, with a step of 2°. For the elevation angle, the antenna is raised from 1° to 5° vertically with the step of 1°. After that, the ergodic method calculates the coverage outcomes from 225 cases in total and obtains the optimal angle by comparing the weak coverage ratio.

Figure 19 shows the optimum angle (azimuth angle: 16° clockwise; elevation angle: 1°) based on the ergodic method. The antenna direction adjustment makes 27 weak coverage points. The weak coverage ratio is reduced by 32.5%. The optimal coverage heatmap of the ergodic method is shown in the Figure 19. Figure 19 displays that the SS-RSRP is significantly enhanced in the red rectangle regions.

Table 7 lists the number of weak coverage points of different methods. In the table, the reference method, method 1, method 2, and method 3 represent the original channel, "RIS + AI" method, manual adjustment, and ergodic method, respectively. According to the Table 7, the

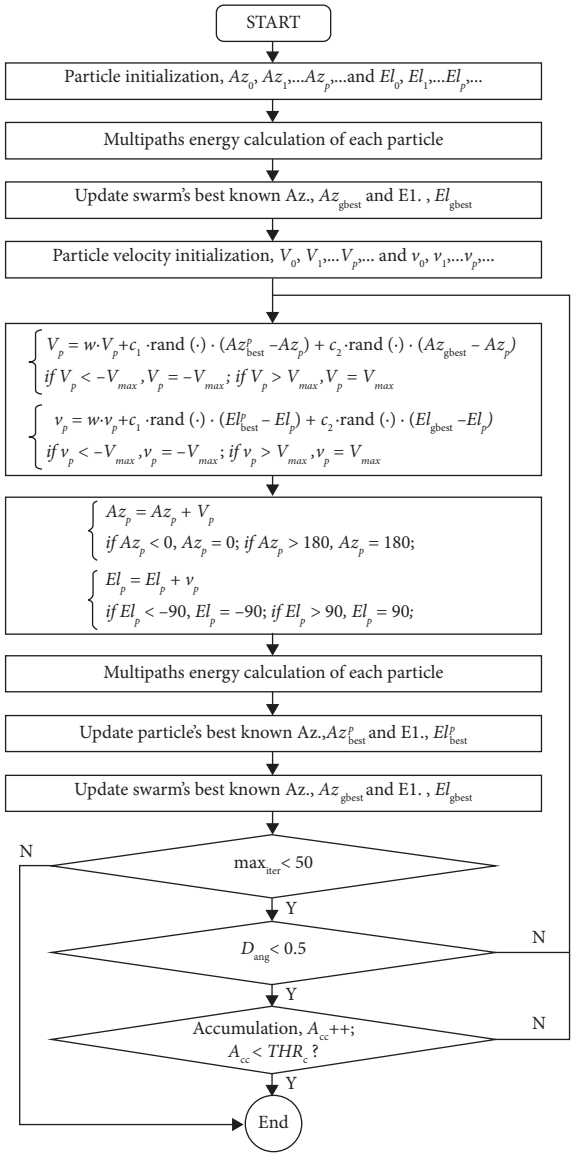

Figure 14: The diagram on the optimal RIS pattern direction selection based on the PSO.

Table 6: PSO parameters configuration.

Parameter name	Configuration data
Swarm	100
Inertia weight, w	0.8
Acceleration constant, c_1	1.5
Acceleration constant, c_2	1.5
Maximum velocity, $V_{\max}$	5°
Minimum velocity, $V_{\min}$	−5°
Convergence threshold, THR_c	3
Maximum iteration, $\max_{iter}$	50

"RIS + AI" method has the least amount of weak coverage points. In the station scenario, some of receiving points with weak coverage have few multipath components with low power. RIS will enhance power of the multipaths for these regions. Consequently, the received power of the original weak coverage region will be improved.

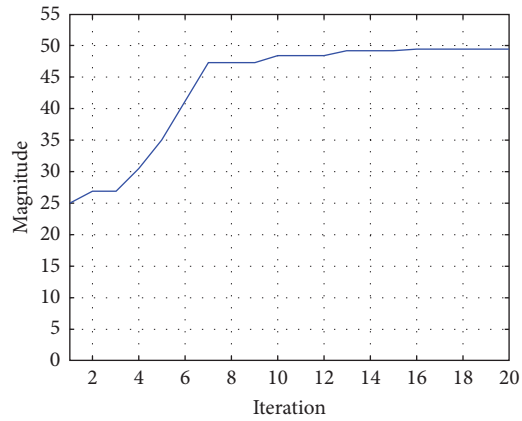

Figure 15: The PSO convergence process.

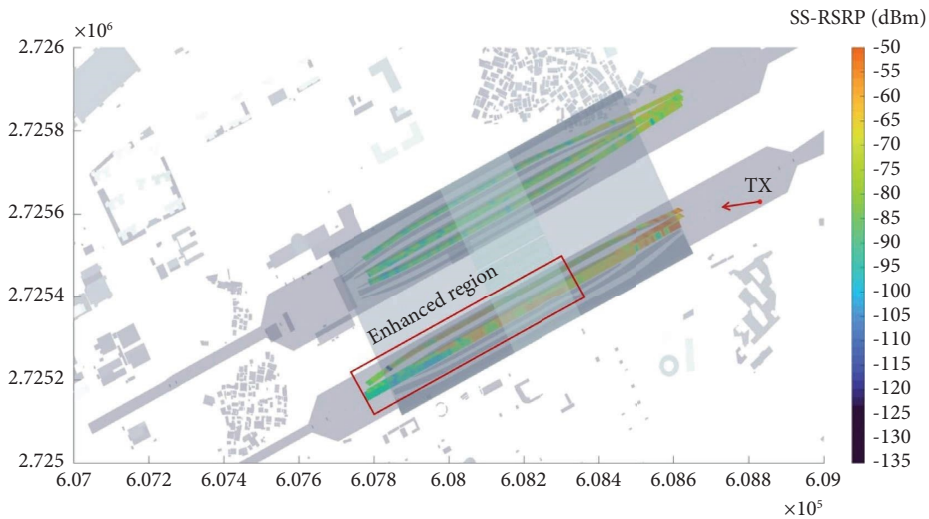

Figure 16: Coverage of the RIS-assisted channel.

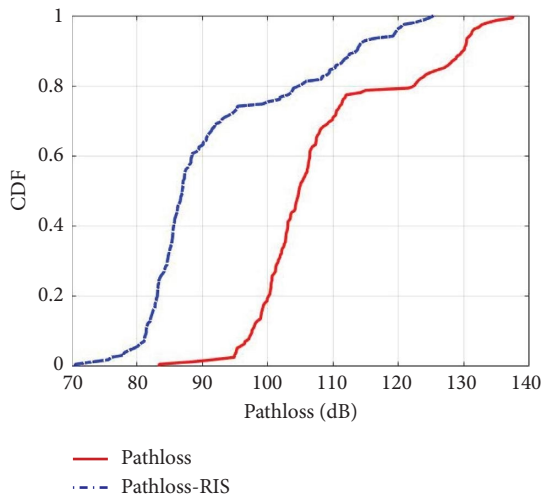

Figure 17: Comparison of RIS-enhanced and original path loss.

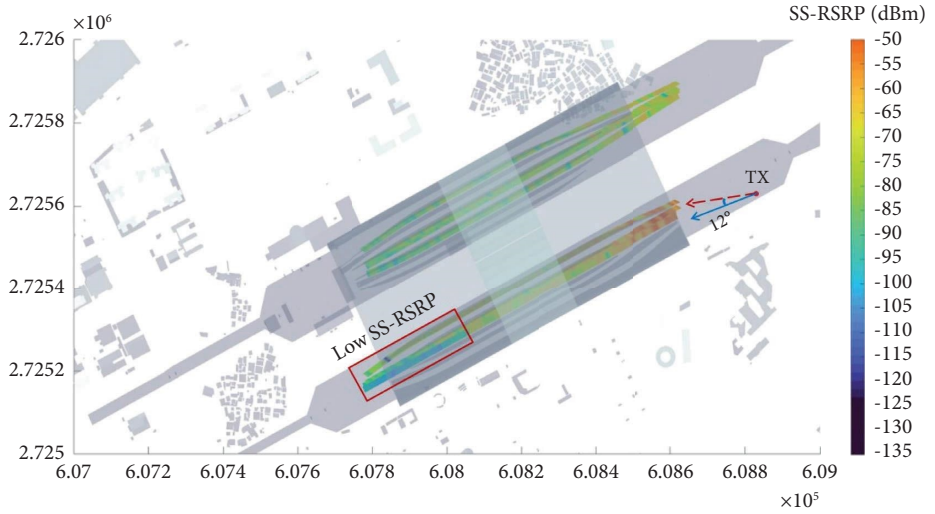

Figure 18: Coverage of manual adjustment channel.

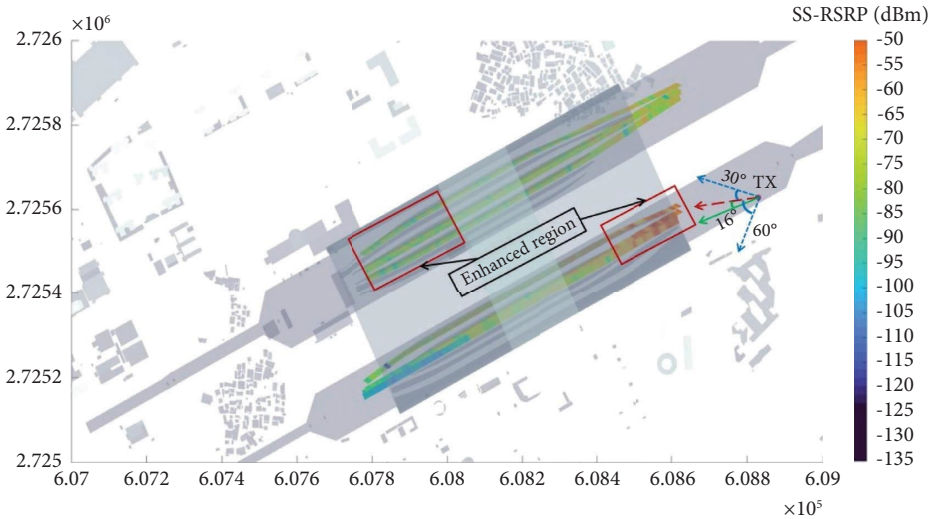

Figure 19: Coverage of ergodic channel.

Table 7: Number of weak coverage points.

Method	Reference method	Method 1	Method 2	Method 3
Number	40	25	37	27

5. Conclusion

In this paper, the HSR station channels at 5G-R band are characterized in terms of path loss, power ratio, and angular spread through RT simulation. The power of the main paths in both the LOS and NLOS regions of the station scenario is compared, which shows a weak power in the NLOS region. Due to the structural characteristic of the scenario, the angular spread of the channel in the horizontal plane is larger than that in the elevation plane. Moreover, there are 5.3% of the receiving points that fail to meet the threshold, which makes it necessary to optimize the network. Compared to most of the previous work, the "RIS + AI" method is innovatively adopted to enhance the coverage. The channel characteristics in the space domain and PSO algorithm is combined to determine the RIS pointing. Upon comparison, the receiving point path loss of the RIS-assisted channel is improved on average by 7.51 dB. The research results of this paper will provide a well reference for the deployment of segmentation scenarios and large-scale promotion of 5G customized networks. In the future research, the fuzzy systems can be considered to describe the networks with more TXs and RISs, and the neural network algorithms can be adopted to solve the optimization.

Data Availability

The datasets generated and analyzed during this study are available from the corresponding author upon request.

Conflicts of Interest

The authors declare that they have no conflicts of interest.

Acknowledgments

The study was supported by the Natural Science Foundation of Hubei Province (2022CFB285) (Project: Research on characteristics of fast time-varying channel of Internet of Vehicles for B5G) and partly supported by 2022 Scientific Research Program of Hubei Provincial Department of Education (no. B2022391).

References

[1] Z. Zhong, K. Guan, W. Chen, and B. Ai, "Challenges and perspective of new generation of railway mobile communications," *ZTE Communications*, vol. 27, no. 04, pp. 44–50, 2021.

[2] C. Li, J. Xie, and W. Gao, "Heterogeneous network access technologies based on 5G-R services for high-speed railway," *ZTE Communications*, vol. 27, no. 04, pp. 18–23, 2021.

[3] Y. Zhao, X. Wang, G. Wang, R. He, Y. Zou, and Z. Zhao, "Channel estimation and throughput evaluation for 5g wireless communication systems in various scenarios on high speed railways," *China Communications*, vol. 15, no. 4, pp. 86–97, 2018.

[4] D. He, B. Ai, M. Schmieder et al., "Influence analysis of typical objects in rural railway environments at 28 ghz," *IEEE Transactions on Vehicular Technology*, vol. 68, no. 3, pp. 2066–2076, 2019.

[5] Q. Tang, K. Guan, Z. Ma, D. Luo, and H. Xu, "Research on wireless signal coverage in urban tunnels based on high-performance ray tracing," *Journal of Beijing Jiaotong University*, vol. 65, no. 4, pp. 1912–1924, 2021.

[6] D. He, B. Ai, K. Guan et al., "Influence of typical railway objects in a mmwave propagation channel," *IEEE Transactions on Vehicular Technology*, vol. 67, no. 4, pp. 2880–2892, 2018.

[7] K. Guan, B. Peng, D. He et al., "Measurement, simulation, and characterization of train-to-infrastructure inside-station channel at the terahertz band," *IEEE Transactions on Terahertz Science and Technology*, vol. 9, no. 3, pp. 291–306, 2019.

[8] Y. Zhao and J. Guo, "An imporved SBR ray-tracing channel simulation method," *Journal of Beijing Jiaotong University*, vol. 45, no. 05, pp. 1–7, 2021.

[9] D. He, B. Ai, K. Guan, L. Wang, Z. Zhong, and T. Kürner, "The design and applications of high-performance ray-tracing simulation platform for 5g and beyond wireless communications: a tutorial," *IEEE Communications Surveys & Tutorials*, vol. 21, no. 1, pp. 10–27, 2019.

[10] Y. Sun, K. An, Y. Zhu, C. Li, and Y. Li, "Intelligent reflecting surface assisted anti-jaming approach for wireless communications," *Chinese Journal of Radio Science*, vol. 36, no. 06, pp. 877–886, 2021.

[11] T. Li, Y. Xu, H. Tong, and K. Pang, "Low-band information and historical data aided non-uniform millimeter wave beam selection algorithm in 5g-r high-speed railway communication scene," *IEEE Transactions on Vehicular Technology*, vol. 71, no. 3, pp. 2809–2823, 2022.

[12] Q. Wu and R. Zhang, "Intelligent reflecting surface enhanced wireless network via joint active and passive beamforming," *IEEE Transactions on Wireless Communications*, vol. 18, no. 11, pp. 5394–5409, 2019.

[13] G. Sun, R. He, B. Ai et al., "A 3d wideband channel model for ris-assisted mimo communications," *IEEE Transactions on Vehicular Technology*, vol. 71, no. 8, pp. 8016–8029, 2022.

[14] Y.-C. Liang, R. Long, Q. Zhang, J. Chen, H. V. Cheng, and H. Guo, "Large intelligent surface/antennas (lisa): making reflective radios smart," *Journal of Communications and Information Networks*, vol. 4, no. 2, pp. 40–50, 2019.

[15] Y. Liu, S. Zhang, F. Gao, J. Tang, and O. A. Dobre, "Cascaded channel estimation for ris assisted mmwave mimo transmissions," *IEEE Wireless Communications Letters*, vol. 10, no. 9, pp. 2065–2069, 2021.

[16] J. An, C. Xu, L. Gan, and L. Hanzo, "Low-complexity channel estimation and passive beamforming for ris-assisted mimo systems relying on discrete phase shifts," *IEEE Transactions on Communications*, vol. 70, no. 2, pp. 1245–1260, 2022.

[17] S. Zeng, H. Zhang, B. Di, Z. Han, and L. Song, "Reconfigurable intelligent surface (RIS) assisted wireless coverage extension: RIS orientation and location optimization," *IEEE Communications Letters*, vol. 25, no. 1, pp. 269–273, 2021.

[18] M. Nemati, J. Park, and J. Choi, "Ris-assisted coverage enhancement in millimeter-wave cellular networks," *IEEE Access*, vol. 8, pp. 188171–188185, 2020.

[19] E. Shtaiwi, H. Zhang, S. Vishwanath, M. Youssef, A. Abdelhadi, and Z. Han, "Channel estimation approach for ris assisted mimo systems," *IEEE Transactions on Cognitive Communications and Networking*, vol. 7, no. 2, pp. 452–465, 2021.

[20] Q. Feng, Y. Lin, M. Shan, and L. Li, "Bessel beam design with coding metasurface," *Chinese Journal of Radio Science*, vol. 36, no. 06, pp. 867–876, 2021.

[21] A. Papazafeiropoulos, Z. Abdullah, P. Kourtessis, S. Kisseleff, and I. Krikidis, "Coverage probability of star-ris-assisted massive mimo systems with correlation and phase errors," *IEEE Wireless Communications Letters*, vol. 11, no. 8, pp. 1738–1742, 2022.

[22] C. Wu, Y. Liu, X. Mu, X. Gu, and O. A. Dobre, "Coverage characterization of star-ris networks: noma and oma," *IEEE Communications Letters*, vol. 25, no. 9, pp. 3036–3040, 2021.

[23] M. Xu, S. Zhang, J. Ma, and O. A. Dobre, "Deep learning-based time-varying channel estimation for ris assisted communication," *IEEE Communications Letters*, vol. 26, no. 1, pp. 94–98, 2022.

[24] R. Zhong, Y. Liu, X. Mu, Y. Chen, and L. Song, "Ai empowered ris-assisted noma networks: deep learning or reinforcement learning," *IEEE Journal on Selected Areas in Communications*, vol. 40, no. 1, pp. 182–196, 2022.

[25] M. Ardashir, M. H. Sabzalian, and W. Zhang, "An interval type-3 fuzzy system and a new online fractional-order learning algorithm: theory and practice," *IEEE Transactions on Fuzzy Systems*, vol. 28, no. 09, pp. 44–50, 2020.

[26] H. Wang, K. A. Alattas, A. Mohammadzadeh, M. H. Sabzalian, A. A. Aly, and A. Mosavi, "Comprehensive review of load forecasting with emphasis on intelligent computing approaches," *Energy Reports*, vol. 8, p. 13, 2022.

[27] Y. Wang, X. Chen, X. Liu et al., "Improvement of diversity and capacity of mimo system using scatterer array," *IEEE Transactions on Antennas and Propagation*, vol. 70, no. 1, pp. 789–794, 2022.

[28] X. Chen, M. Zhao, H. Huang et al., "Simultaneous decoupling and decorrelation scheme of mimo arrays," *IEEE Transactions on Vehicular Technology*, vol. 71, no. 2, pp. 2164–2169, 2022.
[29] K. Guan, B. Peng, D. He et al., "Channel characterization for intra-wagon communication at 60 and 300 GHz bands," *IEEE Transactions on Vehicular Technology*, vol. 68, no. 6, pp. 5193–5207, 2019.
[30] D. H. L. C. Z. Z. Xinghai Guo and K. E. Guan, "Multi-dimensional channel characteristics analysis for avionics compartment," *ZTE Communications*, vol. 27, no. 04, pp. 44–50, 2021.